

Localized measurement of the optical thickness of a transparent window: application to the study of the photosensitivity of organic polymers

Julien Lumeau and Michel Lequime

The development of an optical setup that permits us to carry out high-resolution mappings of the absolute optical thickness of plane-parallel transparent windows is described. This measurement is based on the recording and processing of the spectral transmission of the wafer between 1520 and 1570 nm and has a relative precision better than 10^{-6} . Hence it is used for the characterization of the photosensitivity of two organic photopolymers (cationic ring opening polymer and poly(methylmethacrylate)). The refractive index change dynamics for both materials and the spontaneous evolution of the optical thickness are demonstrated. © 2006 Optical Society of America

OCIS codes: 120.3180, 090.2900.

1. Introduction

Optical thickness is a fundamental parameter to characterize the transmission of optical wafers or solid-spaced Fabry–Perot filters.¹ Different methods such as low-coherence interferometry^{2,3} and confocal microscopy^{4–6} have been widely studied and permit us to perform separate measurements of the mechanical thickness and the refractive index. This paper describes a new method based on interferential spectroscopy, which permits us to carry out mappings of the absolute optical thickness of plane-parallel transparent windows with a relative precision better than 10^{-6} . The range of measurable thickness is equal to [50 μm , 15 mm] and the spatial resolution is between 100 μm and 1 mm. Then, the accuracy of our setup is determined with the characterization of a silica wafer. Finally, this technique is implemented for the characterization of the optical and photosensitive properties of two photopolymers: one is a commercial photopolymer called cationic ring opening polymer

(CROP)^{7,8} and the second one is a photopolymer developed by the Optical Information Group of the California Institute of Technology and is called phenanthrenequinone- (PQ) doped poly(methylmethacrylate) (PMMA).⁹

2. Experimental Description

The optical thickness determination technique that was used in this study is achieved by the interferometric measurement of the transmitted intensity of a wafer at normal incidence. Actually, when a collimated beam is sent through a plane-parallel wafer, multiple reflections occur at the air–glass interfaces. Induced interferences then create a Fabry–Perot cavity, which transmitted intensity (I_T) is given by^{10,11}

$$I_T = \frac{I_0}{1 + F \sin^2[2\pi n(\lambda)t/\lambda]}, \quad (1)$$

where I_0 is the intensity of the incident beam, λ is its wavelength, F is the finesse of the Fabry–Perot etalon, and $n(\lambda)$ and t are, respectively, the refractive index and mechanical thickness of the wafer. If I_0 and F are considered as constant (or are determined experimentally), the transmitted intensity versus the wavelength is finally only a function of the optical thickness of the wafer. In this way, the optical thickness of a wafer can be determined by measuring the transmitted intensity during a spectral sweep. The designed setup is presented in Fig. 1. It is composed of a laser, two distinct optical setups that are labeled

The authors are with the Institut FRESNEL–UMR CNRS 6133, Université Paul Cézanne–EGIM–Université de Provence, Domaine Universitaire de Saint-Jérôme, 13397 Marseille Cedex 20, France. J. Lumeau (jlumeau@creol.ucf.edu) is now with the Photoinduced Processing Laboratory, CREOL, University of Central Florida, P.O. Box 162700, Orlando, Florida 32816-2700.

Received 3 February 2006; accepted 28 March 2006; posted 4 April 2006 (Doc. ID 67782).

0003-6935/06/246099-07\$15.00/0

© 2006 Optical Society of America

Measurement set-up

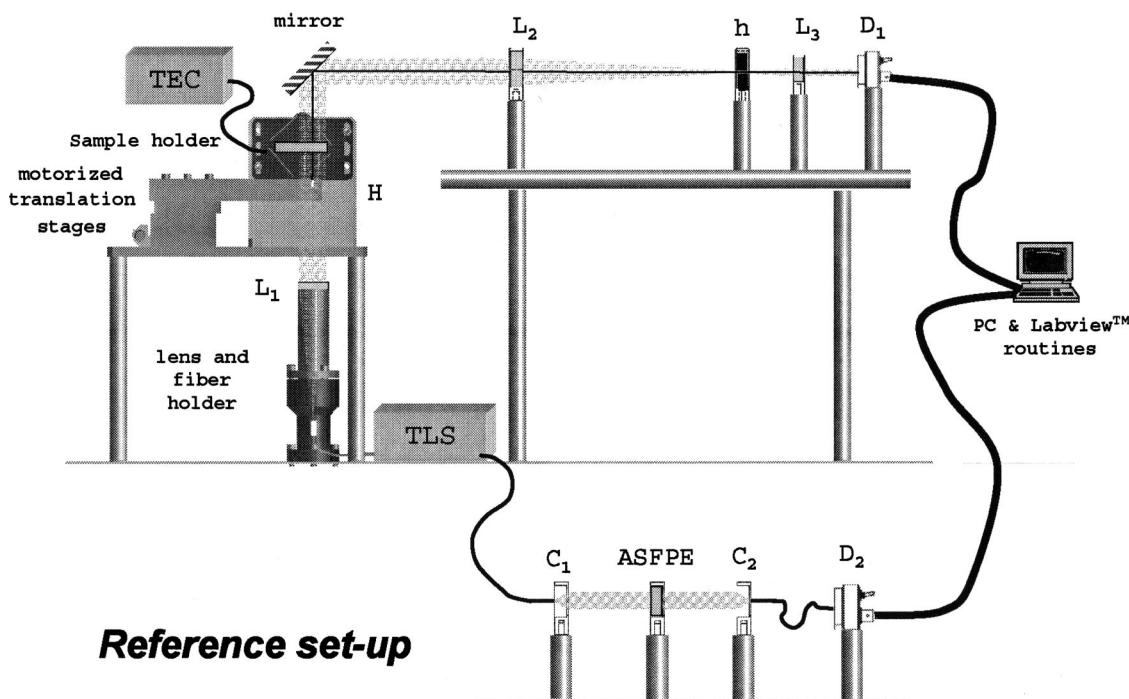


Fig. 1. Schematic of the optical setup used to carry out localized measurements of the optical thickness of transparent windows; L_1 , L_2 , and L_3 , lenses; D_1 and D_2 , InGaAs detectors; h and H , pinholes; TLS, the tunable laser source, ASFPE, an air-spaced Fabry–Perot etalon; and TEC; the thermoelectric controller.

measurement setup and *reference setup*, and a computer to process the acquired signals.

The laser used for this measurement is a tunable EXFO FLS2600 laser source (TLS) that can continuously change its output wavelength from 1520 to 1570 nm with a 10 pm step. The *measurement setup* is first composed with a 120 mm focal length lens (L_1), which collimates the light exiting the output monomode fiber linked to the laser. The sample to be analyzed is positioned on the focal plane of this lens to obtain a magnified image of the fiber. In this way, the whole sample surface is probed without moving it or the fiber tip. A mirror and an afocal system composed of two lenses (L_2 and L_3) are finally added to image the sample on the detector with the correct ratio. With the aim of precisely localizing the measured area, a pinhole (H), whose diameter can vary from 100 μm to 1 mm, is placed just in front of the sample. This pinhole is mounted on x - y motorized translation stages, to be able to scan the probed area.

The goal of our measurement is to carry out stable and repeatable measurements of the local optical thickness. Therefore the sources of instability of our system were studied. The first one is linked to the coherence length of the laser source. Many undesired Fabry–Perot interferometers (FPI) can appear at each glass–air interface. To reduce the influence of these FPI, antireflective coated lenses were used, and any significant parasitic interferometric signal was removed from this system. Moreover, due to the thermal dependence of the optical thickness of the

measured windows, a temperature-controlled sample holder associated with a thermoelectric controller (TEC) was used. This temperature control based on a Peltier effect permits fixing the temperature with a precision and a stability of 0.02 $^{\circ}\text{C}$, and therefore permits reducing thermal variations of the optical thickness to a few angstroms during measurements. Moreover, the temperature of such a sample holder can be changed from 20 $^{\circ}\text{C}$ up to 80 $^{\circ}\text{C}$. Hence the evolution of the optical thickness with temperature can be measured with this setup too, and the thermal coefficient can be calculated from the slope of this curve. Finally, mechanical stability also plays a key role in the accuracy of this measurement; great care was used in the design of this setup such as a vertical probe beam associated with ultrastable mechanics.

Another issue is due to the speed fluctuations of the laser sweep that will induce some nonlinearities of the acquired signal. Accordingly, a specific *reference setup*, which permits performing a calibration between the acquisition's number and the wavelength value during each measurement, was developed. This setup is composed of two monomode fibers ended with Lightpath pigtailed collimators (C_1 and C_2); the first is used for the light emission, and the second is used for the light collection. A Fabry–Perot etalon is positioned in the space between these collimators. Accordingly, for the high-thermal dependence of the standard solid-spaced Fabry–Perot etalons

($\partial n/\partial T \approx 10^{-5}/^{\circ}\text{C}$), a sealed air-spaced Fabry–Perot etalon (ASFPE) is used as a reference. It has a constant free spectral range (FSR) of 100 GHz and a thermal stability of about $-10 \text{ pm}/^{\circ}\text{C}$. The calibration of the wavelength during the sweep of the laser is finally performed by searching the maxima of the ASFPE (whose wavelengths are known) and linearizing the wavelengths between these values. The final precision of the calibration is equal to 1 pm. During each laser sweep, a data acquisition card simultaneously permits the acquisition of the signal of each setup with such a frequency that one acquisition is realized each 10 pm (in accordance with the laser resolution). A typical signal of both setups after calibration is represented in Fig. 2. As can be seen, the signal does not present additional modulations due to parasitic FPI and a good signal-to-noise ratio.

The Airy function that is recorded with the wafer is finally processed to determine the corresponding optical thickness. This last is calculated by optimization with a least-squares method of the model [Eq. (1)] with the measured signal (the refractive index dispersion law is supposed to be known and is set in the theoretical Airy function). However, this merit function not being convex, this determination needs to be tested with several initial solutions to converge to the absolute minimum and not to a local minimum. Finally, this system (laser, translation stages, and signal processing) is computer controlled with LABVIEW and permits us to make automatically optical thickness mappings of plane-parallel windows.

3. Performances

During this measurement, two parameters can have an important effect on the refractive index determination: the parallelism defect between the two faces of the window and the refractive index dispersion of the material. First of all, parallelism will affect the quality of the measured signal. Actually, due to the spatial extension of the beam (between $100 \mu\text{m}$ and 1 mm), the acquired signal is a function of the optical thickness integrated over the whole analysis spot. If the parallelism is not good enough (i.e., greater than several tens of arcseconds), it is possible to show that the contrast of the Airy function will decrease¹² and the precision of the optical thickness determination will also decrease. Therefore ultraparallel windows (i.e., better than 10 arc sec) are needed to reach good accuracy in the determination.

Moreover, during the numerical adjustment between the measured Airy function and the model, the minimum of the merit function will be obtained when¹¹

$$[n'(\lambda_0)T - n(\lambda_0)t] - \lambda_0 \frac{\partial}{\partial \lambda} [n'(\lambda_0)T - n(\lambda_0)t]_{\lambda_0} = 0, \quad (2)$$

where $n(\lambda_0)$ and t are, respectively, the measured refractive index at the wavelength λ_0 and the measured mechanical thickness and $n'(\lambda_0)$ and T are, respectively, the theoretical refractive index at the

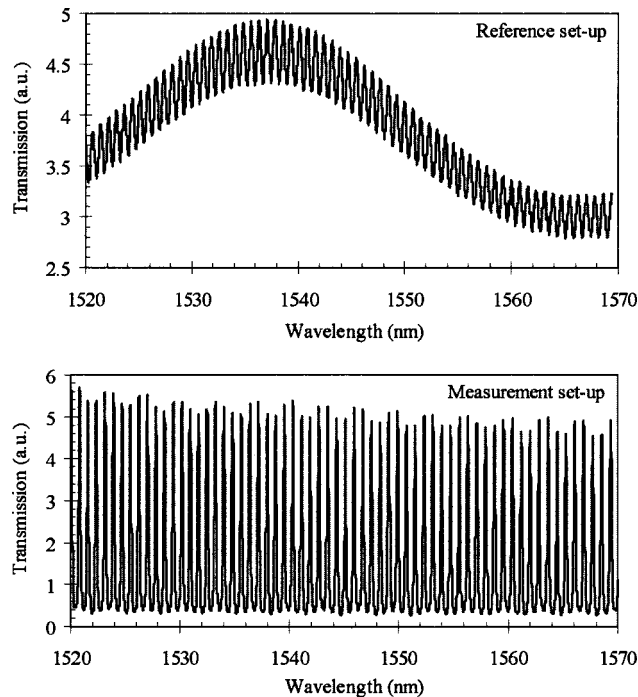


Fig. 2. Typical signals measured on each setup. (Top) Airy function measured with the *measurement setup* in the case of a 1 mm thick silica window. (Bottom) Airy function of the air-spaced Fabry–Perot etalon and measured with the *reference setup*.

wavelength λ_0 and the theoretical mechanical thickness. Therefore the optimization is performed simultaneously on the optical thickness and on the optical thickness dispersion, and the refractive index dispersion law will also play a key role on the measured optical thickness. Hence good knowledge of the dispersion law of the studied material is necessary to obtain an absolute measurement of the optical thickness. However, for some particular materials for which spectral dispersion is unknown, an approximate value of this dispersion can be determined during the fit of the measured signal with the theoretical signal. Actually, if the dispersion law is not injected in Eq. (1), and the experimental curve fit is carried out with a dispersive value of the optical thickness $[ne(\lambda)]$ such as

$$ne(\lambda) = ne_0[1 + b(\lambda - \lambda_0)], \quad (3)$$

where ne_0 and b are two unknown parameters, and λ_0 is the central wavelength (here, 1550 nm); an approximate value of the dispersion (b) can be calculated with this technique by the simultaneous optimization of ne_0 and b . Moreover, it is important to note that this linear approximation is valid, in our case, due to the limited swept wavelength range. But this short range of wavelength also limits the precision of this determination.

Finally, the performances of our optical setup were characterized with a 1 mm thick fused silica window, polished on both sides, having a few arcseconds parallelism. The accuracy of the optical thickness mea-

Table 1. Spectral (δ) and Thermal (b) Constants of CROP and PQ:PMMA Windows

Material	b	δ
CROP	$-7.5 \times 10^{-3} \text{ m}^{-1}$	$5 \times 10^{-4} / ^\circ\text{C}$
PQ:PMMA	$-3.6 \times 10^{-4} \text{ m}^{-1}$	$-2.9 \times 10^{-6} / ^\circ\text{C}$

surement was determined by measuring the optical thickness of this wafer for 72 h. In these conditions, the relative variations of the measured optical thickness were equal to 3×10^{-7} . Afterwards, we tested the dynamic repeatability; that is to say, the relative precision on the optical thickness during mappings. The dynamic repeatability was determined to be better than 10^{-6} . We also tested the ability of this setup to measure the spectral dispersion coefficient (b_{exp}) and the thermal coefficient ($\delta_{\text{exp}} = 1/nt \partial nt / \partial T$). We measured $b_{\text{exp}} = -8.2 \times 10^{-3} \text{ m}^{-1}$ and $\delta_{\text{exp}} = 6.1 \times 10^{-6} / ^\circ\text{C}$ and compared them with the theoretical values: $b_{\text{th}} = -1.2 \times 10^{-2} \text{ m}^{-1}$ and $\delta_{\text{exp}} = 7.3 \times 10^{-6} / ^\circ\text{C}$. Experimental and theoretical values are close to each other. Hence this result demonstrates that this technique can be employed to determine these parameters. However, due to the limited range of wavelengths used for our measurement, the precision of the dispersion coefficient is not optimal (error of $4 \times 10^{-2} \text{ m}^{-1}$ in the case of silica).

Finally, if optical thickness fluctuations are considered to be only due to refractive index changes, and mechanical thickness is considered to be constant (or fluctuations are negligible compared to refractive index variations), we can write that

$$\frac{\Delta nt}{nt} = \frac{\Delta n}{n} + \frac{\Delta t}{t} = \frac{\Delta n}{n}. \quad (4)$$

Thus in the case of photosensitive glasses, refractive index changes can be determined with a precision of approximately 10^{-6} . This note was applied to characterize the photosensitivity of two photopolymers.

4. Measurement of the Photosensitivity of Organic Polymers

A. Precharacterization

The photosensitivity of a commercial polymer called CROP was first characterized with the proposed method. This material, which was developed for holographic data storage applications,^{7,8,13,14} is composed of thin photosensitive polymers (whose thicknesses are between 100 and 300 μm) sandwiched between two parallel antireflective coated BK7 wafers (thicknesses equal to approximately 1.5 mm) forming a very good plane-parallel window. With the refractive indices of the polymers and the wafers being quite identical ($n = 1.52$), negligible reflections can occur at the polymer-BK7 interfaces, and therefore no significant parasitic Fabry-Perot interferometers can appear. Interferential spectroscopy measurements were carried out to demonstrate the

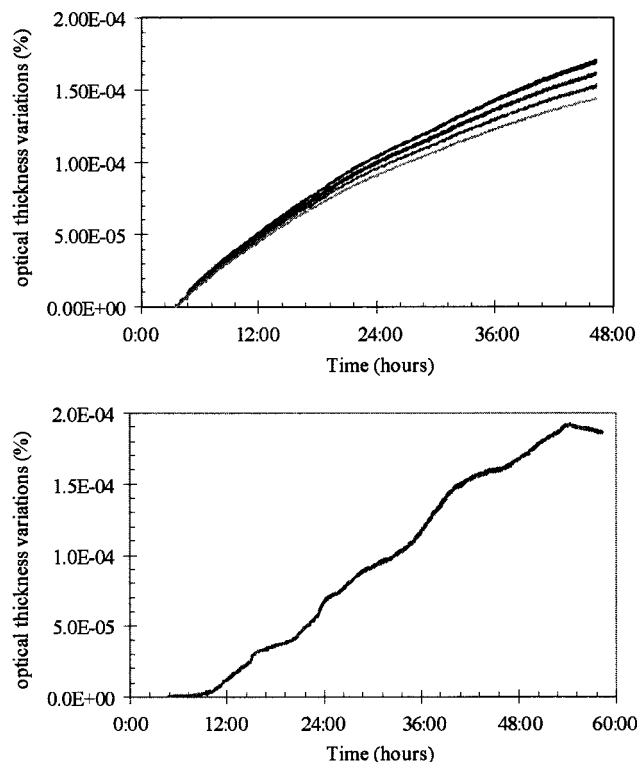


Fig. 3. Evolution of the relative optical thickness variations of a CROP (top graph) and a PQ:PMMA (bottom graph) windows at each of the nine points and without excitation. Demonstration of the spontaneous evolution of the optical thickness with the time that occurs in these polymers.

global optical thickness change dynamics (and therefore, refractive index change dynamics of the photosensitive layer) during material exposure. The second material that was characterized is a photopolymer called PQ-doped PMMA. This photopolymer has been used as a recording material for optical memories and other holographic systems.^{9,15,16} This material consists of a polymeric matrix doped with chromophores, and the PQ molecules have been provided by the California Institute of Technology.

Before studying the photosensitivity of these two materials, spectral dispersion (b_{exp}) and thermal dependence (δ_{exp}), coefficients were measured for each photopolymer. The measured values are summarized in Table 1. We can see that the CROP dispersion is quite identical to the dispersion of fused silica (but this value takes the polymer layer and the BK7 windows into account), and that the dispersion of PQ:PMMA is very small. Concerning the thermal coefficient, the value of the CROP polymer layer contribution was calculated specifically (i.e., the effects of the BK7 windows were canceled by the calculation of the relative contributions). These measurements show that this thermal dependence is very high, and PQ:PMMA has very low thermal sensitivity.

Then, the optical thickness stability of these materials was characterized as a function of time. For each material, the temporal evolution of the optical thickness (without exposure but temperature stabiliza-

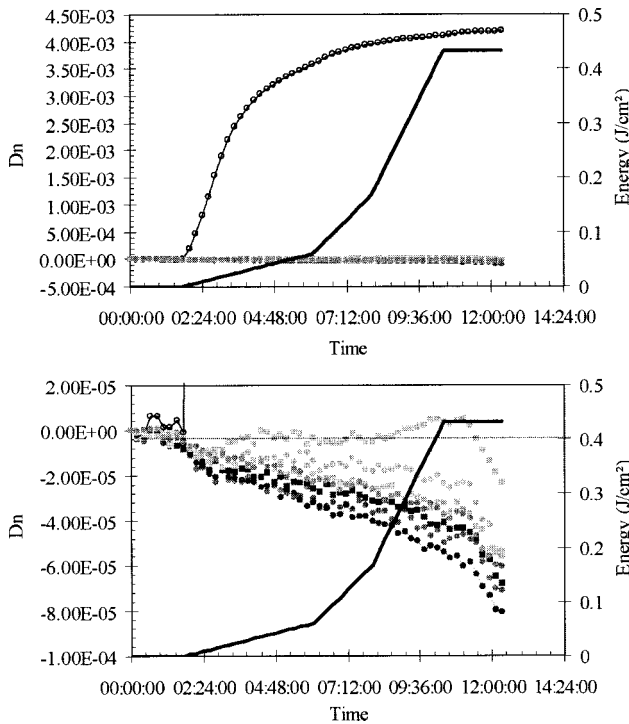


Fig. 4. Evolution of the CROP window refractive index change before, during, and after exposure. Black dots represent this evolution in the excited area and gray dots represent this evolution in the unexposed surrounding media. Finally, the black solid curve represents the increase of energy during the exposure of the material as a function of time.

tion) was measured in a square composed with 3×3 points, the distance between each point being equal to 1.5 mm, and the diameter of the analysis hole being equal to 400 μm . Figure 3 shows that a spontaneous evolution of the optical thickness of the window appears in each material. For the CROP window, this evolution is not identical at each point, and seems to be a diffusionlike effect. With the PQ:PMMA window, the evolution is the same for each point, but contrary to the CROP, this evolution is not monotone. Thus these materials present a high instability for their optical thickness. However, according to the time scale of our photosensitivity measurement (several hours), this spontaneous evolution did not severely affect our photosensitivity characterization.

B. Photosensitivity Characterization

With these two materials being sensitive at 530 nm, the exposure was performed with a GaN LED centered at 525 nm and delivering about 2.5 mW. This LED was then imaged on the sample with a magnification leading to a 1 mm spot size. The refractive index changes were measured with the same strategy described in the study of the evolution of the optical thickness without any exposure (measurement of the optical thickness on 3×3 points all separated by 1.5 mm) and around this area (at the eight peripheral points) before, during, and after exposure. Figure 4 presents the refractive index change measured in

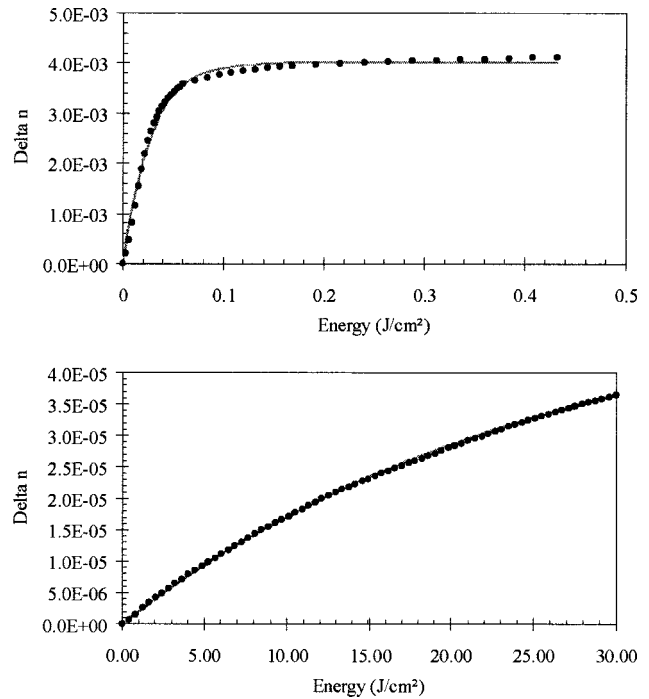


Fig. 5. Evolution of refractive index change versus energy (in J/cm^2) of a CROP (on the top) and a PQ:PMMA (on the bottom) windows. Black dots represent measured data and the gray solid curve represents its fit.

CROP plates. In the first graph (top) of Fig. 4, the refractive index change in the exposed area is shown. This evolution corresponds to the classical variations obtained with photosensitive materials; that is, a linear increase at the beginning of the excitation. When energy exceeds $30 \text{ mJ}/\text{cm}^2$, a decrease of the material sensitivity starts to appear. Finally, the refractive index change saturates at about 4.1×10^{-3} . The value determined with this new technique is quite identical to the refractive index change that was specified by the manufacturer, Aprilis ($\Delta n = 4 \times 10^{-3}$), and which was determined by measuring the diffraction efficiency of a saturated Bragg grating (i.e., when the refractive index is modulated). Therefore this result tends to prove that the main effect producing the refractive index change is a CROP-like polymerization effect and that the diffusion of monomers into the polymer matrix from the unexposed to the exposed area (due to a gradient of monomers that appears during the CROP polymerization) is much less efficient. In the second graph (bottom) of Fig. 4, the evolution of the peripheral points (i.e., the eight unexposed points) is pointed out. During exposure, the refractive index in the surrounding media changes and shows different behaviors according to the measured area. These different evolutions are due to an error in the centering of the excitation beam (i.e., each point was not equidistant to the edge of the excited area). Therefore the behavior of the unexposed surrounding material depends on the distance to the exposure beam. Moreover, these different evolutions showcase that even if the diffusion of the monomers from the unexposed area to

Table 2. Characteristic Constants of CROP and PQ:PMMA Photosensitivity

Material	E_0 (J/cm ²)	Δn_0
CROP	0.028	4.1×10^{-3}
PQ:PMMA	15.4	4.3×10^{-5}

the exposed area is not the main effect leading to the global refractive index change, it has, however, a measurable impact on the optical thickness of the unexposed surrounding media.

Similar experiments were carried out with a PQ:PMMA window. Conclusions are quite similar to those obtained with CROP windows but a lower refractive index change was measured. To compare refractive index dynamics, the refractive index change in the CROP and in PQ:PMMA versus energy were represented in Fig. 5. The maximum refractive index change in the PQ:PMMA window was demonstrated to be 100 times lower than in the CROP windows. The sensitivity of PQ:PMMA is also lower than in the CROP. To quantify this sensitivity difference, these

two curves were fitted with a classical diffusion law such as

$$\Delta n(E) = \Delta n_0 \left[1 - \exp\left\{-\frac{E}{E_0}\right\}\right], \quad (5)$$

where $\Delta n(E)$ is the refractive index change during exposure with an energy density E (in J/cm²), Δn_0 is the maximum refractive index change, and E_0 is a characteristic energy describing the material sensitivity. The main parameters were determined and are presented in Table 2. These data demonstrate that the sensitivity of PQ:PMMA is 500 times lower than the CROP sensitivity.

Finally, a mapping of the exposed area of a CROP window was carried out with a smaller hole diameter (100 μm). The optical thickness was measured before and after exposure (100 mJ/cm²). Afterward, the local refractive index change was calculated from these two measurements (Fig. 6). This experiment demonstrates that refractive index change almost perfectly reproduces the shape of the exciting beam. However, an enhancement of the refractive index change equal to several 10^{-4} appears on the edge of the excited area. This enhancement is additional evidence and a quantification of the diffusionlike effect, which is due to the diffusion of monomers from the unexposed to the exposed area.

5. Conclusions

What we believe is a new method based on interferential spectroscopy was demonstrated. This method permits us to carry out ultraprecise mappings of the optical thickness of a transparent window. Such a measurement is based on Fabry–Perot interferometry and needs the use of a tunable laser. Precharacterization with a silica window demonstrated that the relative precision of this technique is better than 10^{-6} . Therefore the optical thickness of 1 mm thick windows can be determined with precision better than 1 nm using this method. Then, the photosensitivity of the two photopolymers (CROP and PQ:PMMA) was measured. The refractive index change dynamics under LED exposure at 530 nm was determined. CROP windows were demonstrated to be 500 times more sensitive than PQ:PMMA windows and lead to refractive index changes two orders of magnitude higher. Finally, we showed that due to the high sensitivity of this technique and its spatial resolution, very small effects such as the impact of monomer diffusion on the refractive index can be measured.

The authors thank J. Mumbru and D. Psaltis of Caltech for providing samples and the technical description of the PQ:PMMA samples that were developed in their laboratories.

References

1. J. Floriot, F. Lemarchand, and M. Lequime, "Double coherent solid-spaced filters for very narrow-bandpass filtering applications," *Opt. Commun.* **222**, 101–106 (2003).
2. M. Haruna, M. Ohmi, T. Mitsuyama, H. Tajiri, H. Maruyama, and M. Hashimoto, "Simultaneous measurement of the phase

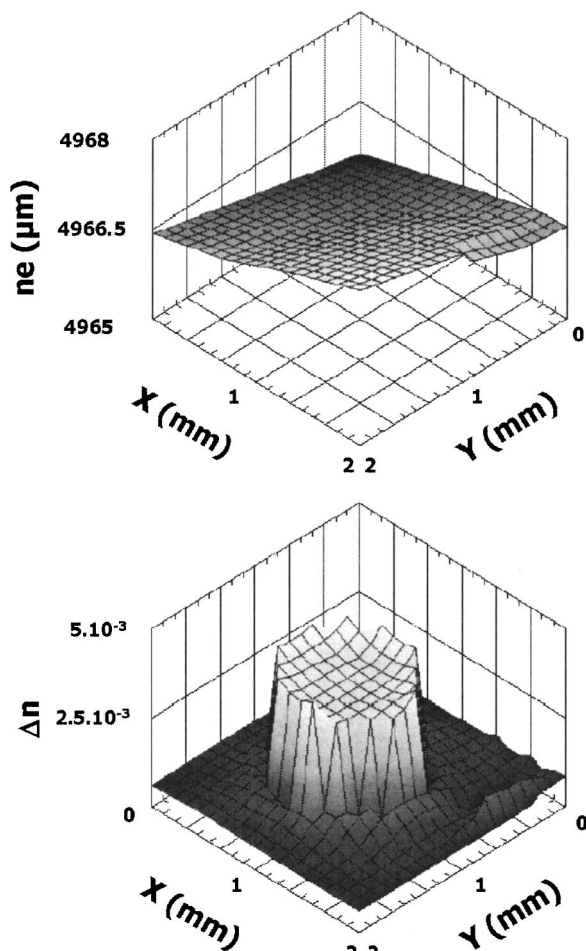


Fig. 6. Mapping of the local optical thickness of a CROP window before exposure (on the top) and of the local refractive index change after exposure (on the bottom).

- and group indices and the thickness of transparent plates by low-coherence interferometry," *Opt. Lett.* **23**, 966–968 (1998).
3. B. L. Danielson and C. Y. Boisrobert, "Absolute optical ranging using low coherence interferometry," *Appl. Opt.* **30**, 2975–2979 (1991).
 4. T. R. Corle, J. T. Fanton, and G. S. Kino, "Distance measurements by differential confocal optical ranging," *Appl. Opt.* **26**, 2416–2420 (1987).
 5. I. K. Ilev, R. W. Waynant, K. R. Byrnes, and J. J. Anders, "Dual-confocal fiber-optic method for absolute measurement of refractive index and thickness of optically transparent media," *Opt. Lett.* **27**, 1693–1695 (2002).
 6. T. Fukano and I. Yamaguchi, "Separation of measurement of the refractive index and the geometrical thickness by use of a wavelength-scanning interferometer with a confocal microscope," *Appl. Opt.* **38**, 4065–4073 (1999).
 7. Aprilis Incorporated, http://www.aprilisinc.com/holographic_media.htm.
 8. R. T. Ingwall and D. Waldman, "CROP photopolymer for hologram recording," SPIE's International Technical Group Newsletter **11**, 2 (2000).
 9. S. H. Lin and K. Y. Hsu, "Bulk photopolymer with negligible shrinkage for holographic memory," SPIE's International Technical Group Newsletter **11**, 2, 5, 10 (2000).
 10. H. A. Macleod, *Thin-Film Optical Filters*, 3rd ed. (Institute of Physics Pub., 2001).
 11. Doric Lenses Incorporated, http://www.doriclenses.com/PDF/NOT_FPE_ENG.pdf.
 12. H. R. Giovannini, S. J. Huard, and M. R. Lequime, "Influence of chromatic dispersion on a dual-wavelength passive-homodyne detection method for fiber-coupled interferometers," *Appl. Opt.* **33**, 2721–2733 (1994).
 13. D. M. Sykora and M. Morris, "Photopolymer characterization and grating playback at telecommunication wavelength," presented at the Diffractive Optics and Micro-Optics Topical Meeting, Tucson, Arizona, 3–5 June 2002.
 14. L. Paraschis, "Volume holographic recording utilizing photo-initiated polymerization for nonvolatile digital data storage," Ph.D. thesis (Stanford University, 2000).
 15. J. Mumburu, I. Solomatine, D. Psaltis, S. H. Lin, K. Y. Hsu, W. Chen, and W. T. Whang, "Comparison of the recording dynamics of phenanthrenequinone-doped poly(methyl methacrylate) materials," *Opt. Commun.* **194**, 103–108 (2001).
 16. G. J. Steckman, I. Solomatine, G. Zhou, and D. Psaltis, "Characterization of phenanthrenequinone-doped poly(methyl methacrylate) for holographic memory," *Opt. Lett.* **23**, 1310–1312 (1998).